Sustaining the DC Micro-Grid Bus Voltage through the Implementation of Finite Control Sets Model Predictive Control in a Photovoltaic Converter System

Wakhyu Dwiono[1,2], Bambang Riyanto Trilaksono[1*], Tri Desmana Rachmildha[1] and Arwindra Rizqiawan[1]

[1]School of Electrical Engineering and Informatics, Institut Teknologi Bandung, Bandung, Indonesia
[2]Department of Electrical Engineering, Universitas Muhammadiyah Purwokerto, Purwokerto, Indonesia
Corresponding author:[*] bambang.riyanto@itb.ac.id

Abstract: The escalating cost-effectiveness of photovoltaic (PV) panels has amplified their allure for integration into DC micro-grids as indispensable devices for harvesting clean energy sources. Typically, the PV system operates in Peak Power Point Tracing (PPPT) mode, extracting the highest energy to supply the micro-grid. The converter within the energy storage system assumes a pivotal role in distributing power, facilitating power-sharing, and sustaining the stability of the DC bus voltage. Consequently, any disruption in this converter system poses a critical risk, potentially compromising the stability of the DC micro-grid and leading to system failure. Beyond maximizing solar energy extraction, PV systems can contribute to bus voltage stability through proper treatment. This strategy guarantees system stability during brief energy storage system failures, contingent upon sufficient sunlight radiation conditions to support the load. Despite various methods proposed in the literature for sustaining bus voltage using PV systems, there remains a need to enhance the time response of these systems for faster performance. This paper addresses this concern by proposing a modification to the objective function variable applied in Finite Control Sets Model Predictive Control (FCS MPC). The objective function, obtained from the Integral Absolute Error (IAE) of the PV inductor current, contrasts with the current set-point derived from integrating the PV step-up converter's output voltage error. The efficacy of the proposed method is validated through simulation and experimentation, demonstrating its capability to sustain the bus voltage even in the absence of the energy storage system converter.

Keywords: DC bus voltage maintaining, FCS MPC, DC micro-grid

1. Introduction

Owing to the diminishing expenses and escalating efficacy of PV panels, they are progressively emerging as a compelling choice for the provision of electrical energy [1], particularly in regions distant from the primary grid. In such circumstances, the established electric grid assumes the character of an autonomous micro-grid [2], capable of operating in either direct current (DC) or alternating current (AC) configurations.

An inherent benefit of PV panels lies in their generation of DC electrical energy, facilitating seamless integration into DC micro-grid systems without necessitating immense conversion. Furthermore, DC systems present numerous benefit over their AC counterparts, including the absence of frequency synchronization, harmonics, and reactive power issues, as underscored in earlier scholarly investigations [2] – [4]. Therefore, there is a notable scholarly interest in devising methodologies to effectively incorporate PV panels into DC micro-grid systems.

To mitigate the sporadic occurrence of sunlight energy, the conventional approach involves integrating PV panels with energy storage systems. Two primary methods exist for connecting PV systems to energy storage systems: firstly, by interfacing them with the low-voltage DC bus [5] – [7] and subsequently linking to the micro-grid's DC bus; secondly, by directly paralleling them on the micro-grid's DC bus [8] – [17]. In the earlier scenario, PV panels harness energy

Received: January 20th, 2023. Accepted: December 1st, 2023
DOI: 10.15676/ijeei.2023.15.4.5

under optimal circumstances when the micro-grid faces power deficits, at the same time the energy storage converter system upholds the DC bus voltage. Contrarily, during instances of surplus power in the micro-grid, PV panels can be deployed in a voltage-regulation mode in conjunction with the energy storage converter system [5], [9] – [17].

Within the published-works, diverse methodologies exist for governing PV systems in DC micro-grids. The scholars in [9] and [10] have introduced an enhancement to droop control by incorporating secondary control. In [9], the researchers opted for voltage control in operating PV and established set-points that account for voltage fluctuations and load currents. Nevertheless, simulation outcomes revealed that despite these efforts, power fluctuations in the PV system still impacted the voltage of the DC bus. Conversely, in [10], the scholars employed PV in PPPT mode, yet the approach remained untested in the context of fluctuations in sunlight energy. In [11], a secondary control was proposed, albeit solely applied to PV systems operating under voltage-regulation conditions akin to those presented in [9]. Notably, the distinction lies in the fact that the set-point used in the secondary control exclusively considers alterations in load power.

In their work documented in [12], the authors introduced a proportional-integral (PI)-based controller employing a dual-loop structure for the PV system, omitting the inclusion of droop as the PV operates in PPPT mode. Nevertheless, it is imperative to note that the proposed system has not undergone comprehensive testing to date, primarily due to the omission of an assessment regarding the micro-grid power conditions, whether they are in a state of oversupply or undersupply.

In [13] - [15], control systems are posited that hinge on the specific utilizing mode of the system. In the case of [13], the PV system transitions from PPPT to a fixed power mode. While this system exhibits effective performance with a meticulously scrutinized reliability, it is worth noting that the control algorithm becomes increasingly intricate with the expansion of the system's scale. A parallel strategy is presented in [14], where the system's utilizing mode is contingent upon factors such as PV power production, load, and state of charge (SoC) of the energy storage. However, the reliability of this system necessitates further meticulous analysis. The implementation of a strategy focused on consistently maximizing photovoltaic (PV) power extraction through PPPT is detailed in reference [15]. DC bus voltage regulation is accomplished through the utilization of battery converters and super capacitors. The incorporation of a Proportional-Integral (PI) controller facilitates the maintenance of DC bus voltage regulation, even in the presence of load variations and fluctuations in sunlight irradiance. It is important to note, however, that the system's performance has not been thoroughly scrutinized under conditions of surplus power supply.

Mitigating minimal energy storage usage is a focal point in both [16] and [17]. In [16], the researchers deploy PV in PPPT and voltage-regulation mode, with mode transitions contingent upon the hysteresis value of the bus voltage error relative to the set-point. This configuration enables proper system functionality, even in the absence of energy storage availability. Nevertheless, notable overshooting occurs during load changes. Conversely, in [17], the authors advocate for adaptable power point tracing in PV systems and employ direct model predictive control (MPC) for energy storage systems, aiming to curtail energy storage consumption by optimizing the utilization of PV resources. It is important to highlight that the system in [17] has not undergone testing in scenarios involving energy storage system collapse.

This paper, which is an extended version of [18], introduces a refined objective function variable, incorporated as a control loop for the PV control within the framework of FCS-MPC, drawing inspiration from [19] and [20]. To substantiate the efficacy of the proposed controller, its application is realized on a basic boost converter topology, selected for its switching dynamics despite its lower efficiency compared to other topologies [21].

The primary objective of the proposed method is to sustain the DC micro-grid bus voltage, even in the event of energy storage fail, by enhancing the system's response speed and mitigating overshoot. The efficacy of this proposed method is substantiated through Matlab simulations. The subsequent sections of this paper are structured as follows: Section 2 expounds on the dynamics of the step-up converter system, Section 3 elucidates the details of the proposed control system, Sections 4 and 5 delve into the simulation and experimentation results, and Section 6 provides a comprehensive summary of conclusions and outlines avenues for future research.

2. Step-up Converter

A schematic representation of a basic isolated DC micro-grid system is represented in Fig.1, comprising a PV system as the principal energy source, complemented by an energy storage system for backup and loads. To streamline the analysis, this study employs a step-up converter with a current source output for both the PV and energy storage systems, as depicted in Fig.2. The operation of the step-up converter within a PV system is unidirectional and involves two discernible states, denoted as i_{Lp} for inductor current and v_{o1} for output voltage. Three parameters characterize this system, specifically L_p, r_{Lp}, and C_1, illustrating the inductor, inductor resistance, and capacitor, respectively. It is notable that switch S_1 is controllable, whereas switch S_2 is non-controllable in this particular configuration.

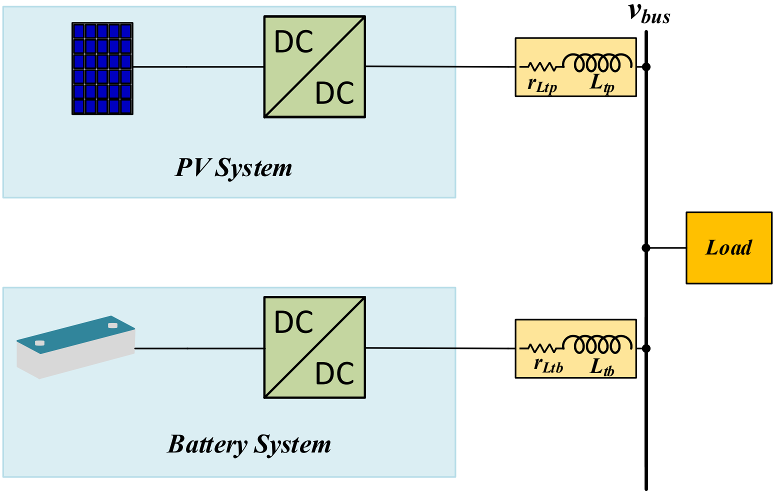

Figure 1. A basic DC micro-grid is composed of a load, a PV system, and an energy storage system.

On the contrary, the step-up converter employed in the energy storage system functions bi-directionally, manifesting two distinct states denoted as i_{Lb} for inductor current and v_{o2} for output voltage. This system is characterized by three parameters: L_b, r_{Lb}, and C_2, signifying the inductor, inductor resistance, and capacitor, successively. Importantly, it is observed that both switches, S and $\bar{S}$, are controllable within this specific system.

$$\frac{d}{dt}\begin{bmatrix} i_{Lp} \\ v_{o1} \end{bmatrix} = \begin{bmatrix} \frac{-r_{lp}}{L_p} & 0 \\ 0 & 0 \end{bmatrix}\begin{bmatrix} i_{Lp} \\ v_{o1} \end{bmatrix} + \begin{bmatrix} \frac{1}{L_p} & 0 \\ 0 & \frac{-1}{C_1} \end{bmatrix}\begin{bmatrix} v_{pv} \\ i_{o1} \end{bmatrix} \tag{1a}$$

$$\frac{d}{dt}\begin{bmatrix} i_{Lp} \\ v_{o1} \end{bmatrix} = \begin{bmatrix} \frac{-r_{lp}}{L_p} & \frac{-1}{L_p} \\ \frac{1}{C_1} & 0 \end{bmatrix}\begin{bmatrix} i_{Lp} \\ v_{o1} \end{bmatrix} + \begin{bmatrix} \frac{1}{L_p} & 0 \\ 0 & \frac{-1}{C_1} \end{bmatrix}\begin{bmatrix} v_{pv} \\ i_{o1} \end{bmatrix} \tag{1b}$$

$$\frac{d}{dt}\begin{bmatrix} i_{Lb} \\ v_{o2} \end{bmatrix} = \begin{bmatrix} \frac{-r_{lb}}{L_b} & 0 \\ 0 & 0 \end{bmatrix}\begin{bmatrix} i_{Lb} \\ v_{o2} \end{bmatrix} + \begin{bmatrix} \frac{1}{L_b} & 0 \\ 0 & \frac{-1}{C_2} \end{bmatrix}\begin{bmatrix} v_{batt} \\ i_{o2} \end{bmatrix} \tag{2a}$$

$$\frac{d}{dt}\begin{bmatrix} i_{Lb} \\ v_{o2} \end{bmatrix} = \begin{bmatrix} \frac{-r_{lb}}{L_b} & \frac{-1}{L_b} \\ \frac{1}{C_2} & 0 \end{bmatrix}\begin{bmatrix} i_{Lb} \\ v_{o2} \end{bmatrix} + \begin{bmatrix} \frac{1}{L_b} & 0 \\ 0 & \frac{-1}{C_2} \end{bmatrix}\begin{bmatrix} v_{batt} \\ i_{o2} \end{bmatrix} \tag{2b}$$

The step-up converter systems for both the PV and energy storage exhibit turn-on and turn-off modes. The dynamics of the step-up converter governing the PV system are articulated in (1a) and (1b) for the turn-on and turn-off modes, successively. Correspondingly, the dynamic equations for the turn-on and turn-off modes of the energy storage step-up converter system are represented by (2a) and (2b).

3. Proposed Control Approach

This section delves into the discussed control approach for FCS-MPC, employing an adjusted objective function inspired by earlier studies, as documented in [17] and [18]. The adapted objective function is designed for application in both the step-up converter controller for the photovoltaic system (FCS MPC1) and the energy storage system (FCS MPC2). The control system block diagram is presented in Fig.3.

For the FCS MPC to depend on anticipated model values for forthcoming steps, it is imperative to discretize the dynamic equations governing both the PV step-up converter system (expressed in (1a) and (1b)) and the energy storage (articulated in (2a) and (2b)). The discretization process is accomplished through Euler integration, employing a sampling period denoted as T_s.

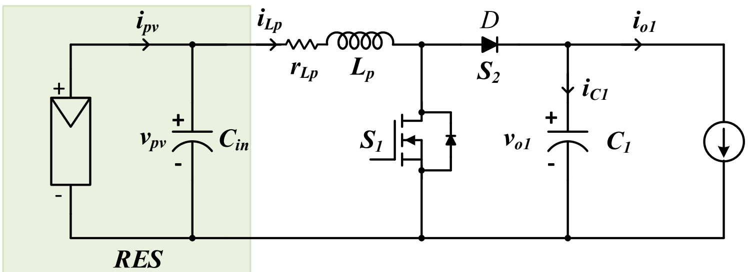

(a)

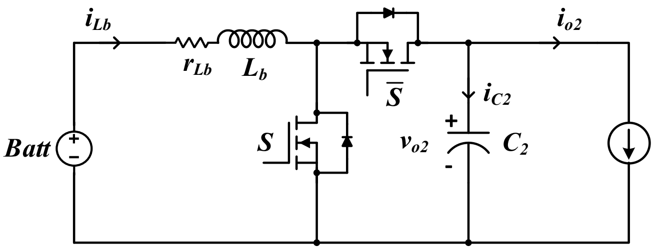

(b)

Figure 2. (a). Step-up converter for PV system (b) Bidirectional step-up converter for the energy storage system.

As follows are the dynamic equations for the PV step-up converter system:

$$x(k+1) = Ap_1 x(k) + Bp_1 in_p(k) \quad (3a)$$
$$x(k+1) = Ap_2 x(k) + Bp_2 in_p(k) \quad (3b)$$

Where $x(k) = [i_{Lp} \quad v_{o1}]^{\top}$ is explained as state vector, $in_p(k) = [v_{pv} \quad i_{o1}]^{\top}$ is explained as input vector and the calculation of the matrices Ap_1, Ap_2, Bp_1 and Bp_2 are as follows: $Ap_1 = I_2 + \begin{bmatrix} \frac{-r_{lp}T_s}{L_p} & 0 \\ 0 & 0 \end{bmatrix}$, $Ap_2 = I_2 + \begin{bmatrix} \frac{-r_{lp}T_s}{L_p} & \frac{-T_s}{L_p} \\ \frac{T_s}{C_1} & 0 \end{bmatrix}$ and $Bp_1 = Bp_2 = \begin{bmatrix} \frac{T_s}{L_p} & 0 \\ 0 & \frac{-T_s}{C_1} \end{bmatrix}$. I_2 is an identity matrix with dimensions of 2x2.

The following holds for the dynamic equation of the energy storage step-up converter system:

$$x(k+1) = Ab_1 x(k) + Bp_1 in_b(k) \quad (4a)$$
$$x(k+1) = Ab_2 x(k) + Bb_2 in_b(k) \quad (4b)$$

Where $x(k) = [i_{Lb} \quad v_{o2}]^{\top}$ is explained as state vector, $in_b(k) = [v_{batt} \quad i_{o2}]^{\top}$ is explained as input vector and the calculation of the matrices Ab_1, Ab_2, Bb_1 and Bb_2 are as follows: $Ab_1 = I_2 + \begin{bmatrix} \frac{-r_{lb}T_s}{L_b} & 0 \\ 0 & 0 \end{bmatrix}$, $Ab_2 = I_2 + \begin{bmatrix} \frac{-r_{lb}T_s}{L_b} & \frac{-T_s}{L_b} \\ \frac{T_s}{C_2} & 0 \end{bmatrix}$ and $Bb_1 = Bb_2 = \begin{bmatrix} \frac{T_s}{L_b} & 0 \\ 0 & \frac{-T_s}{C_2} \end{bmatrix}$. I_2 is an identity matrix with dimensions of 2x2.

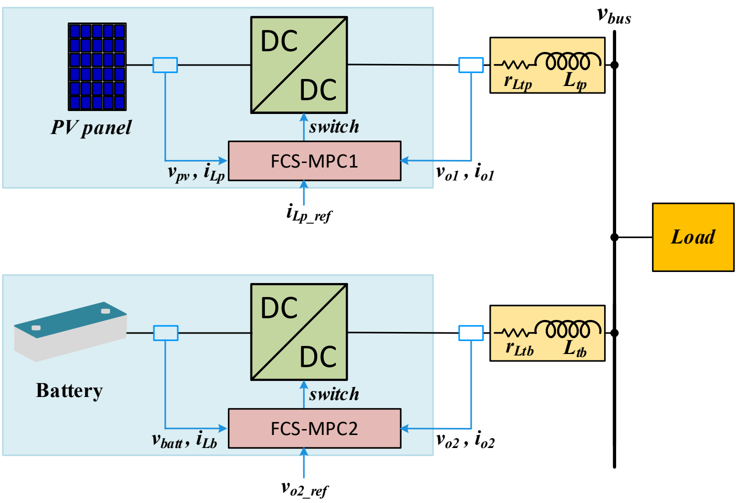

Figure 3. Proposed PV control system.

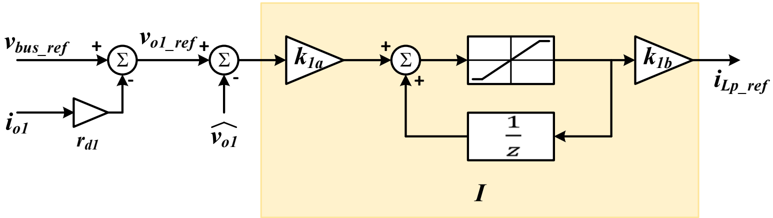

Figure 4. Control loop for i_{Lp_ref}.

The objective functions for FCS MPC1 and FCS MPC2 are established on the IAE criterion, incorporating an adjusted set-point signal. Equation (5) delineates the objective function for FCS MPC1, where the set-point signal (pertaining to the PV inductor current) is produced through the integral control of output voltage error, as depicted in Fig.4. This set-point signal is juxtaposed with the predicted PV inductor current, and subsequently, the absolute error between i_{Lp_ref} and $\widehat{i_{Lp}}$ is employed to compute the IAE for the ensuing N_p steps.

$$\begin{aligned} J(k) &= \frac{1}{N_p}\left\{\sum_{n=1}^{N_p}\left|i_{Lp\_ref} - \widehat{i_{Lp}}(n)\right|\right\} \\ &= \frac{1}{N_p}\left\{\sum_{n=1}^{N_p} f_{e1}\right\} \end{aligned} \tag{5}$$

Equation (6) illustrates the objective function for FCS MPC2, utilizing an output voltage set-point signal produced by the control loop depicted in Fig.5. Concurrently, the set-point for the energy storage inductor current is obtained from the load power projection [18], as represented in (7).

$$\begin{aligned} J(k) &= \frac{1}{N_p}\left\{\sum_{n=1}^{N_p}\left|i_{Lb\_ref} - \widehat{i_{Lb}}(n)\right| + \left|v_{o2\_ref} - \widehat{v_{o2}}(n)\right|\right\} \\ &= \frac{1}{N_p}\left\{\sum_{n=1}^{N_p} f_{e2}\right\} \end{aligned} \tag{6}$$

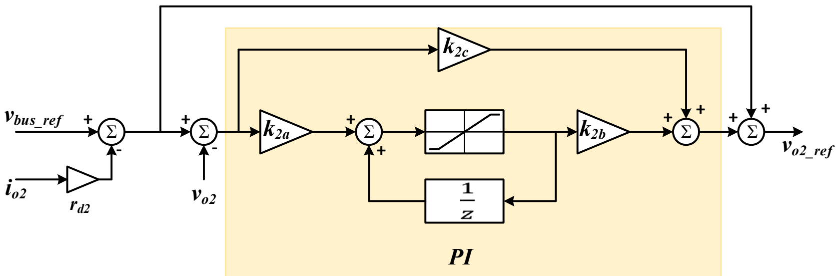

Figure 5. Loop control for v_{o2_ref}.

Table 1. Algorithm of the FCS-MPC

```
Require: l = 1,2,3,⋯,2^{N_p}, u*(k) = 1, U(l,N_p), x(k), J*(k) = ∞
    l = 1
    while l < 2^{N_p} do
        x̂(1) = x(k), starting value of x̂
        J = 0, starting value of the cost
        for n = 1 → N_p do
            u(n) = U(l;n)
            calculate x̂(n+1), using (3a) and (3b) or (4a) and (4b)
            J = J + f, f = f_e1 or f_e1, using (5) or (6)
        end for
        if J < J*(k) then
            J*(k) = J
            u*(k) = u(n)
        end if
        l = l + 1
    end while
```

$$i_{Lb_{ref}} = \frac{(v_{o2\_ref})^2 i_{o2}}{v_{batt} v_{o2}} + a\left(v_{o2\_ref} - \widehat{v_{o2}}\right) \quad (7)$$

The algorithmic depiction of the control operation is presented in Table 1. To commence the control procedure, all conceivable combinations of switching sequences, denoted as $U(l, N_p)$, are initially devised. The prediction horizon, N_p, dictates the total number of switching patterns. At time k, measurements are taken for the system states $x(k)$, input voltage, and load current. Predictions for the subsequent N_p steps are then calculated, based on the dynamics aligned with the input switching patterns previously prepared. During each horizon step, the cost (J) is computed for a specific switching pattern. Subsequently, the total costs for each switching pattern are compared to identify the lowest cost ($J^*(k)$). The first switching combination ($u^*(k)$) associated with this lowest cost is then applied to the converter.

4. Simulation Results

This section presents a computer simulation study to validate the efficacy of a proposed control approach for the PV step-up converter system. The designed method aims to sustain the DC bus voltage of the micro-grid, especially in instances where the energy storage step-up converter system is interrupted and unable to fulfill its part in voltage regulation. The simulation, executed using Matlab Simulink over a 5-second duration, involves providing a bus voltage set-point (v_{bus_ref}) of 120 volts to each controller. Figures 7 to 9 delineate the response of the proposed controller (depicted by the blue line) in comparison to the response of the linear quadratic regulator (LQR) represented by the red line. The energy storage system was disabled between 1.5 to 3.5 seconds throughout all three scenarios. Sunlight irradiance (depicted in Fig. 6) and loading patterns for each scenario are presented in Table 2. Parameters for the two system blocks are detailed in Table 3. The inductor value is carefully chosen to guarantee a highest input current and output voltage ripple of about 1%, accommodating a power capacity of around 1 kW. The transmission line parameter is inspired by [6]. Controller parameters are established using the Zigler-Nichols tuning procedure.

Table 2. Sunlight Irradiance and Load Pattern

Scenario	Irradiance	Initial Load	Load Shift 1[a]	Load Shift 2[b]
1	Fig 6	425 W	(425 to 850) W	(850 to 425) W
2	Fig 6	360 W	(360 to 720) W	(720 to 360) W
3	1000 W/m2	425 W	(425 to 850) W	(850 to 425) W

[a] at 2 seconds
[b] at 3 seconds

Table 3. Block System Parameters

Parameter	PV System	Energy Storage System
v_{in}	$v_{open\_circuit}$ =74.6 V	36 V
L	L_p=5mH	L_b=5mH
r_L	r_{Lp}=40mΩ	r_{Lb}=40mΩ
C	C_{o1}=560μF	C_{o2}=560μF
L_t	L_{tp}=0.22mH	L_{tb}=0.22mH
r_{Lt}	r_{Ltp} = 0.6Ω	r_{Ltb} = 0.6Ω
k	k_{1a}=0.5, k_{1b}=0.0081	k_{2a}=1e-4, k_{2b}=1, k_{2c}=1
r_d	r_{d1}=0.1	r_{d2}=0.2
N_p	4	4
a	-	a =0.1
Limiter	±1500	±50

T_s = 1/20000 s, PV=1000 W_p

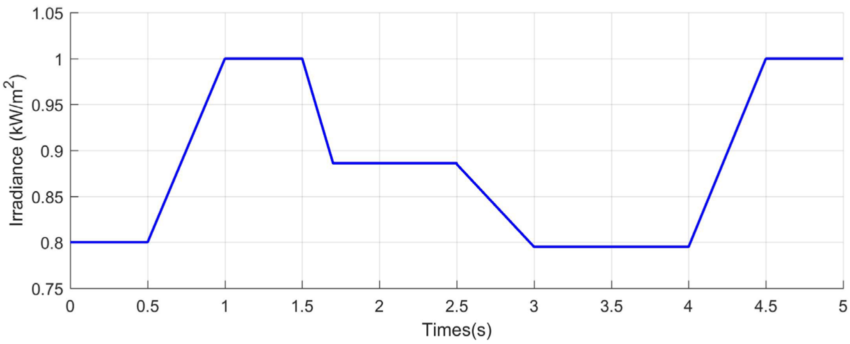

Figure 6. Irradiance pattern used in the simulation

The system responses in the three scenarios (depicted in Fig. 7 and detailed in Tables 4 to 6) reveal that the response time of the PV inductor current to load variations is swift, with a rise time of 0.5 seconds. Upon connecting the energy storage system, the v_{bus} voltage reaches the nominal value v_{bus_ref}, specifically at 119.1 volts. The discrepancy between v_{bus} and v_{bus_ref} arises from a voltage drop along the transmission line, as the controller utilizes the voltage measured at the converter's output. In the presence of the energy storage, the current supplied to the load by the PV surpasses that from the energy storage due to the lower PV r_{droop} (r_{d1}) compared to the energy storage r_{droop} (r_{d1}).

Figure 7a illustrates the outcomes for scenario 1, where the initial load is set at 34 Ω, corresponding to 425 watts. Initially, the v_{bus} voltage attains 119.13 volts. Upon deactivating the energy storage, the v_{bus} voltage experiences a marginal decline to 118.59 volts. Even with a load alteration to 17 ohms, equivalent to 850 watts, the bus voltage is sustained at 114.92 volts, signifying a 4.23% decrease from the nominal value.

Table 4. Simulation Result Data at 1 Second

Scenario	i_{Lp} (A)	i_{Lb} (A)	P_{pv}(W)	v_{bus} (V)
1	4.17	3.64	303.41	119.13
2	3.54	3.10	259	119.16
3	4.19	3.79	304.42	119.10

Table 5. Simulation Result Data at 1.75 Seconds

Scenario	i_{Lp} (A)	i_{Lb} (A)	P_{pv}(W)	v_{bus} (V)
1	6.32	0	446.77	118.59
2	5.28	0	377.45	118.82
3	6.25	0	446.95	118.64

Table 6. Simulation Result Data at 2.5 Seconds

Scenario	i_{Lp} (A)	i_{Lb} (A)	P_{pv}(W)	v_{bus} (V)
1	9.24	0	612.76	114.92
2	8.18	0	559.65	118.6
3	9.21	0	631.72	115.81

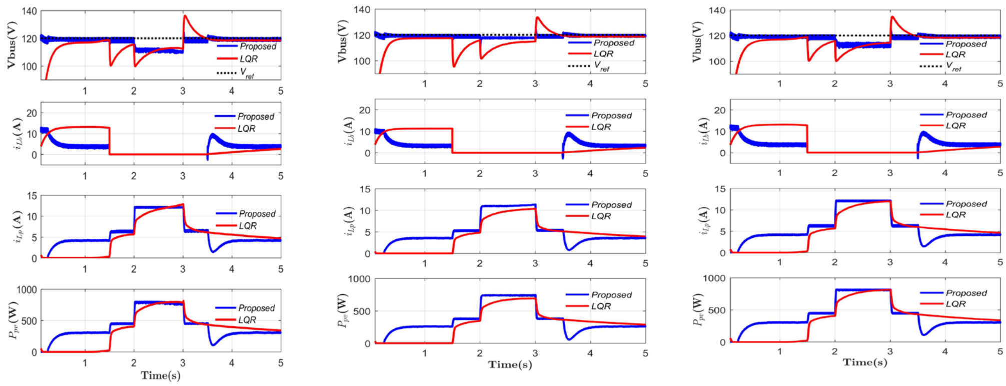

(a) (b) (c)

Figure 7. System response: a) scenario 1, b) scenario 2, c) scenario 3

Scenario 2, depicted in Fig. 7b, utilizes the same irradiance pattern as Scenario 1. The distinguishing factor between the two lies in the load variation for Scenario 2, transitioning from 40 Ω (equal to 360 watts) to 20 Ω (equal to 720 watts). In contrast to Scenario 1, the load in Scenario 2 is lower. Consequently, with the energy storage disabled, the v_{bus} voltage can be upheld at 118.82 volts. Furthermore, even with the load adjusted to 20 Ω, the v_{bus} remains at 118.6 volts, marginally surpassing the v_{bus} value observed in Scenario 1. A v_bus value of 118.6 volts signifies a 1.17% decrease from the nominal voltage.

Figure 7c exhibits the outcomes of Scenario 3, characterized by a consistent irradiance level of 1000 W/m². This scenario replicates the load conditions from Scenario 1. As the load transitions to 17 ohms, the v_{bus} voltage rises to 115.81 volts, signifying a 3.5% reduction from the nominal value. This voltage increment is attributed to the substantial and constant sunlight irradiance, a departure from the fluctuating irradiance observed in Scenario 1. A comparative analysis of the three scenarios reveals that the v_{bus} voltage experiences a magnitude overshoot of 4.2% during the transition from a heavy to a light load (17 Ω to 34 Ω or 20 Ω to 40 Ω).

As depicted in Fig.7, it is evident that the efficacy of the proposed controller outperforms that of the LQR. The outcomes illustrate a swifter response, diminished percentage overshoot, and the maintenance of the bus voltage in proximity to the set-point value, even in the absence of the energy storage connection. Additionally, the proposed controller capitalizes on the PV panel to supply a greater amount of power compared to the energy storage.

5. Experiment Results

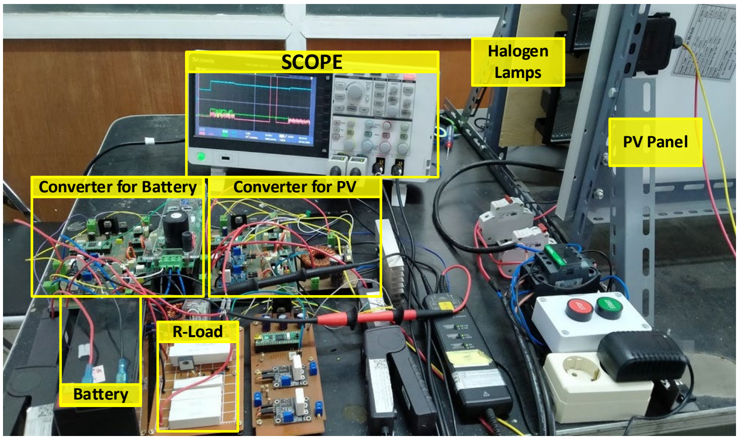

Figure 8. Experimental set-up of a simple DC microgrid

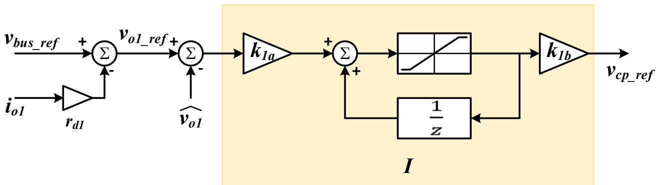

Figure 9. Adjusted loop control for v_{cp_ref}.

The experiment was conducted utilizing a circuit featuring an identical block diagram to the simulations. The experimental configuration is illustrated in Fig.8. The control system for both the PV converter and the energy storage is executed on a mini32 board (specifically, the PIC32MX534F064H model), a product manufactured by Mikroe. Notably, the parameter values of the circuit components align with the physical conditions observed within our laboratory, as detailed in Table 7.

When applying the control system in the simulation to the mini32 board, which runs at the maximum system clock frequency of 80 MHz, it becomes evident that a single iteration of the control process demands a significant computational time, approximately equivalent to 1/3000 of a second. Consequently, when deployed for direct switching within a PV system, the controller needs to improve in achieving an output power level close to its maximum capacity. As a result, a strategic modification was introduced to the control system. While the control algorithm retained the FCS-MPC framework, the formulation of the cost function was adjusted. Specifically, (8) was tailored for PV systems, and (9) for energy storage systems, which are depicted in Fig.9 and Fig. 10. These equations are calculated based on the prediction of system dynamics concerning variations in the duty cycle value. The adjusted algorithm is outlined in Table 8, and the selected duty cycle value is subsequently fed into the PWM generator register on the PIC32MX. This uncomplicated algorithm draws inspiration from the fixed-frequency switching approach introduced in prior works [22]-[24]. The block diagram for generating set-points for the PV FCS-MPC and Energy storage is also adjusted, as shown in Fig.9 and 10.

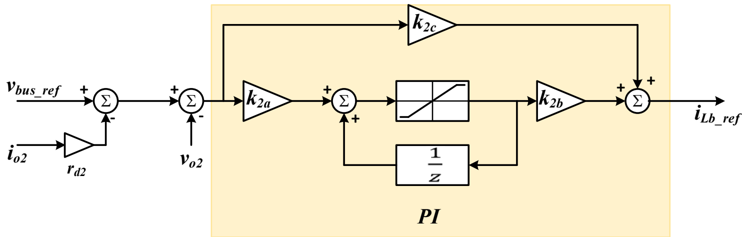

Figure 10. Adjusted loop control for i_{Lb_ref}.

$$J(k) = \left|v_{cp\_ref} - \widehat{v_{cp}}(n)\right| \quad (8)$$

$$J(k) = \left|i_{Lb\_ref} - \widehat{i_{Lb}}(n)\right| \quad (9)$$

The parameters for the FCS-MPC controller are documented in Table 9. The LQR controller, already incorporating state integral error, was designed based on the small signal model of each step-up converter system, utilizing a weighting matrix represented as Q =[1 0 0; 0 1 0; 0 0 10], along with R=10. The experiment spanned 28 seconds and involved the following specifics:

- The set-point voltage, v_{bus_ref}, was set at 40 volts.
- The system was activated at 3.5 seconds, introducing a load of 27 watts.
- At the 10-second mark, the energy storage system was disconnected, carrying a load of 35 watts.
- Subsequently, at 24.5 seconds, the energy storage system was reconnected, supporting a 27-watt load.

Table 7. Experimental step-up converter parameters

Parameter	PV System	Energy storage System
v_{in}	$v_{open\_circuit}$ =21.6 V	12 V
L	L_p=1mH	L_b=1mH
r_L	r_{Lp}=0.22 Ω	r_{Lb}=0.22 Ω
C	C_{o1}=470μF	C_{o2}=470μF
L_t	L_{tp} = 0	L_{tb} = 0
r_{Lt}	r_{Ltp} = 0.5 Ω	r_{Ltb} = 0.5 Ω

Table 8. Adjusted FCS-MPC algorithm

Require: $d = [d_1, d_2, d_3, \ldots, d_N]$, Ts, J_{min}=100000, x_k= $[i_{Lp}\ v_c]^T$, $n=1$
while $n < N+1$ **do**
Compute the dynamic when switch is ON
$x_{k+1} = A_1\ x_k + B_1\ u$, for $t = d_n T_s$
shifting the states value, $x_k = x_{k+1}$
Compute the dynamic when switch is OFF
$x_{k+1} = A_2\ x_k + B_2\ u$, for $t = (1 - d_n)T_s$
Compute $J(n)$
if $J(n) < J_{min}$
$J_{min} = J(n)$
$i_{min} = n$
end if
end while
Duty-cycle PWM = $d(i_{min})$

Table 9. Experimental controller parameters

Parameter	PV System	Energy storage System
k	k_{1a}= 0.5 , k_{1b}=0.05	k_{2a}= 0.1, k_{2b}= 2.5
r_d	r_{d1} = 1	r_{d2} = 4
N_p	1	1
Limiter	±1500	±180

T_s = 1/2500 s, PV=50 W_p, Irradiance=6x500W (halogen lamps)

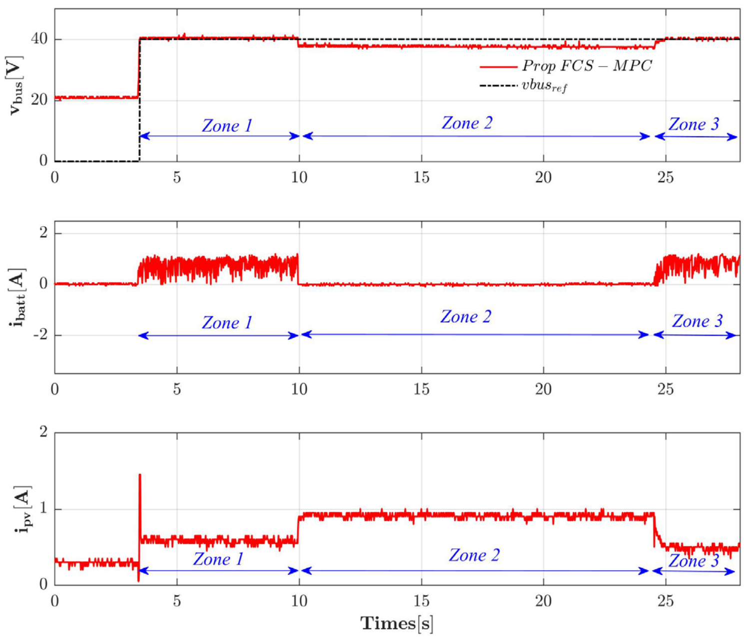

Figure 11. Experimental system response

The system's response of the proposed FCS-MPC control system throughout the experiment is visually represented in Figure 11. The temporal progression of the experiment has been demarcated into three distinct intervals. Zone 1 spans the time interval from 3.5 to 10 seconds. Zone 2 is defined between the 10th and 24.5-second marks, and Zone 3 encompasses time durations exceeding 24.5 seconds.

Figure 11 illustrates that the proposed FCS-MPC controller swiftly responds to the specified set-point value and promptly adapts to changing conditions, such as load increments or energy storage converter system disconnections. In Zone 1, where the installed load is 27 watts, the FCS-MPC controller demonstrates the capability to bring the v_{bus} state near its designated set-point value at about 40.3 volts, as indicated in Table 10. This bus voltage is achieved with an RMS ripple value of 0.48 volts, corresponding to approximately 1.2%. Upon entering Zone 2, characterized by an installed load of 35 watts (equivalent to 70% of PV power capacity) with the energy storage system disconnected, the FCS-MPC controller exhibits the ability to maintain the bus voltage at a level of 37.6 volts, representing 94% of the set-point value. The RMS ripple value in this scenario amounts to 0.32 volts or approximately 0.85%. Upon reconnection of the energy storage system with a load of approximately 27 watts, the bus voltage is reinstated to 40.1 volts, accompanied by an RMS ripple of 0.24 volts, constituting roughly 0.6%.

Figure 12 offers a comparative analysis of the system response between the FCS-MPC control system (red line) and the Linear Quadratic Regulator (LQR) control system (blue line) when subjected to load variations and energy storage system disconnection over a duration spanning from 7.5 to 20 seconds. Notably, Figure 12 reveals that while the LQR control system can maintain the bus voltage equal to v_{bus_ref} when the energy storage system is disconnected, it is visually evident that voltage and current ripples are considerably prominent. In Zone 1, the bus voltage and the PV current ripple measure 0.57 volts and 0.18 amperes, while in Zone 2, the corresponding values are 0.41 volts and 0.14 amperes (as presented in Table 11). A distinguishing characteristic of the FCS-MPC control system's response is that it exhibits significantly reduced PV current ripple, approximately one-third of what is observed with the LQR control system.

Table 10.FCS-MPC system’s states response

Value	Zone 1			Zone 2			Zone 3		
	v_{bus} (V)	i_{Lbatt} (A)	i_{Lpv} (A)	v_{bus} (V)	i_{Lbatt} (A)	i_{Lpv} (A)	v_{bus} (V)	i_{Lbatt} (A)	i_{Lpv} (A)
Mean	40.3	0.76	0.58	37.6	-	0.91	40.1	0.84	0.5
Ripple	0.48	0.27	0.05	0.32	-	0.03	0.24	0.28	0.03

Table 11. LQR system’s states response

Value	Zone 1			Zone 2		
	v_{bus} (V)	i_{Lbatt} (A)	i_{Lpv} (A)	v_{bus} (V)	i_{Lbatt} (A)	i_{Lpv} (A)
Mean	40.7	0.55	0.65	40.2	-	1.1
Ripple	0.57	0.16	0.18	0.41	-	0.14

Based on the outcomes derived from this experimentation, it becomes evident that the proposed FCS-MPC controller can uphold bus voltage at its set-point value when the energy storage system is disconnected. Furthermore, it accomplishes this with a reduced ripple component compared to the LQR control system. This condition enhances the advantages of the FCS-MPC controller due to sustaining the reliability and performance of the PV system during the sunlight energy harvesting process.

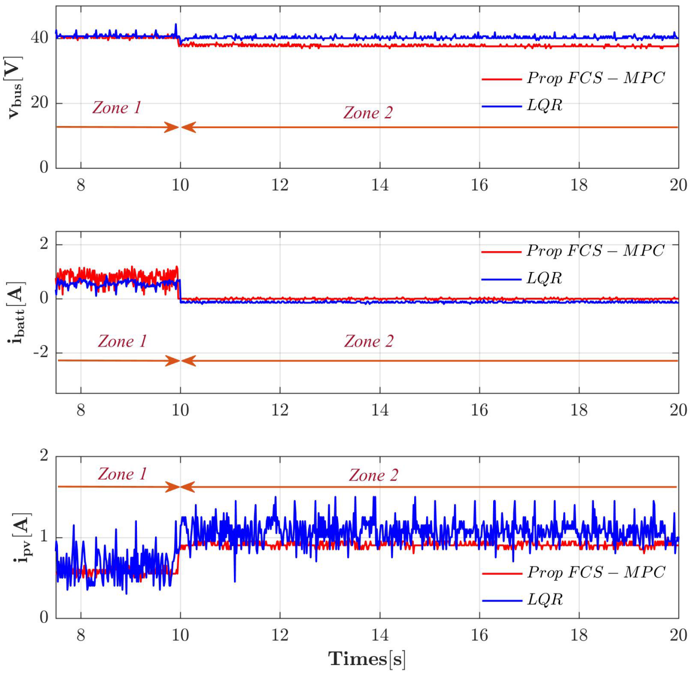

Figure 12. Comparison the FCS-MPC system response to the LQR.

6. Conclusion

This paper has demonstrated that the proposed FCS-MPC is capable of effectively sustaining the DC bus voltage close to its specified set-point value, even when the energy storage system is disconnected from the network.

The simulation outcomes unequivocally reveal that the proposed control methodology significantly contributes to the sustaining of the micro-grid bus voltage, even in scenarios where the energy storage step-up converter system is non-operational. The control system effectively maintains the bus voltage at a level 4.23% below the nominal value, even with the energy storage system switched off and a load of 850 watts. Moreover, the observed overshoot during load transitions, specifically from 17 Ω to 34 Ω (equal to 850 watts to 425 watts) or from 20 Ω to 40 Ω (equal to 720 watts to 360 watts), is minimal, registering at 4.2%. In reaction to load adjustments, the system exhibits a quick response time of about 0.5 seconds.

Notably, while experimental results suggest that the LQR control system outperforms the FCS-MPC controller in sustaining bus voltage under conditions of energy storage system disconnection, the FCS-MPC controller exhibits the distinct advantage of generating reduced PV current ripples compared to the LQR system. This feature presents a noteworthy advantage, as the minimized PV current ripple plays a pivotal role in safeguarding the reliability and performance of the PV system during the sunlight energy harvesting process. Further exploration of computational efficiency within this controller, including overcoming the issue of constant power loads, also conducting a comparative analysis to assess the effectiveness of FCS-MPC control in comparison to similar methodological approaches, such as the safe ball algorithm [25], is a promising avenue for prospective research.

7. Acknowledgement

The authors extend their appreciation to the LPDP, The Ministry of Finance of the Republic of Indonesia, for their financial support in funding this research.

8. References

[1] Haegel, Nancy M. and Kurtz, Sarah R. "Global Progress Toward Renewable Electricity: Tracking the Role of Solar," *IEEE Journal of Photovoltaics*, vol. 11, no. 6 pp. 1335-1342, Nov. 2021, doi: 10.1109/JPHOTOV.2021.3104149.

[2] Arash M. Dizqah, Alireza Maheri, Krishna Busawon, Peter Fritzson, "Standalone DC microgrids as complementarity dynamical systems: Modeling and applications," Control Engineering Practice, vol. 35, pp.102-112, 2015, https://doi.org/10.1016/j.conengprac.2014.10.006.

[3] W. Bai, M. Sechilariu, and F. Locment, "DC Microgrid System Modeling and Simulation Based on a Specific Algorithm for GridConnected and Islanded Modes with Real-Time Demand-Side Management Optimization," Applied Sciences, vol. 10, no. 7, p. 2544, 2020, https://doi.org/10.3390/app10072544.

[4] Pedro J. dos Santos Neto, Tarcio A.S. Barros, Joao P.C. Silveira, Ernesto Ruppert Filho, Juan C. Vasquez, "Power management techniques for grid-connected DC microgrids: A comparative evaluation, " Applied Energy, vol. 269, p. 115057, 2020, https://doi.org/10.1016/j.apenergy.2020.115057.

[5] M. Nasir, Z. Jin, H. A. Khan, N. A. Zaffar, J. C. Vasquez and J. M. Guerrero, "A Decentralized Control Architecture Applied to DC Nanogrid Clusters for Rural Electrification in Developing Regions," in IEEE Transactions on Power Electronics, vol. 34, no. 2, pp. 1773-1785, Feb. 2019, doi: 10.1109/TPEL.2018.2828538.

[6] Salem Batiyah, Roshan Sharma, Sherif Abdelwahed and Nasibeh Zohrabi, "An MPC-based power management of standalone DC microgrid with energy storage," International Journal of Electrical Power and Energy Systems, vol.120, pp.105949, 2020, https://doi.org/10.1016/j.ijepes.2020.105949.

[7] Muhammad Zakir, Hadeed Ahmed Sher, Ammar Arshad, Matti Lehtonen, "A fault detection, localization, and categorization method for PV fed DC-microgrid with power-sharing management among the nanogrids," International Journal of Electrical Power and Energy Systems, vol.137, pp.107858, 2022, https://doi.org/10.1016/j.ijepes.2021.107858.

[8] Eko Adhi Setiawan, Novagia Adita, "Hybrid nanogrids development to improve residential reliability and resiliency supply: Testing and implementation," Energy Reports, vol.8, pp.284-290, 2022, https://doi.org/10.1016/j.egyr.2022.01.060.

[9] Y. Wu and H. Li, "DC Microgrid Droop Control with Voltage and Current Dual Compensation," 2022 4th International Conference on Electrical Engineering and Control Technologies (CEECT), Shanghai, China, pp. 1274-1278, 2022, doi: 10.1109/CEECT55960.2022.10030392.

[10] R. Ranjan, A. Panchbhai and A. Kumar, "Decentralized Primary Control of PV-Battery System Integrated With DC Microgrid in Off-Grid Mode," 2022 IEEE International Conference on Power Electronics, Smart Grid, and Renewable Energy (PESGRE), Trivandrum, India, pp. 1-5, 2022, doi: 10.1109/PESGRE52268.2022.9715964.

[11] J. Ni, B. Zhao, A. Goudarzi, Y. Li and J. Xiang, "A Dispatchable Droop Control Method for PV Systems in DC Microgrids," in IEEE Access, vol. 11, pp. 7588-7598, 2023, doi: 10.1109/ACCESS.2023.3237591.

[12] R. D. Bhagiya and R. M. Patel, "PWM based Double loop PI Control of a Bidirectional DC-DC Converter in a Standalone PV/Battery DC Power System," 2019 IEEE 16th India Council International Conference (INDICON), Rajkot, India, pp. 1-4, 2019, doi: 10.1109/INDICON47234.2019.9028974.

[13] Tsai-Chi Kuo, Trang Thi Pham, Duong Minh Bui, Phuc Duy Le, Tan Luong Van, Po-Tsang Huang, "Reliability evaluation of an aggregate power conversion unit in the off-grid PV-battery-based DC microgrid from local energy communities under dynamic and transient operation," Energy Reports, vol.8, pp. 5688-5726, 2022, https://doi.org/10.1016/j.egyr.2022.03.190.

[14] M. V. Satya Sai Chandra, B. D. B, L. V. Kumar and S. Mohapatro, "Voltage Control and Energy Management of Solar PV fed Stand-alone Low Voltage DC Microgrid for Rural Electrification," 2020 21st National Power Systems Conference (NPSC), Gandhinagar, India, pp. 1-6, 2020, doi: 10.1109/NPSC49263.2020.9331911.

[15] Seger, Ali & Khosroabadi, Saeed. “Study and Treat the Effect of Loads and Radiation Changes for the Standalone Photovoltaic System by a Hybrid Storage System”. International Journal on Electrical Engineering and Informatics. 13. 813-827. 10.15676/ijeei.2021.13.4.4.

[16] V. Fernao Pires, Armando Cordeiro, Daniel Foito, J. Fernando Silva, ”Control transition mode from voltage control to MPPT for PV generators in isolated DC microgrids,” International Journal of Electrical Power and Energy Systems, pp. 107876, 2022, https://doi.org/10.1016/j.ijepes.2021.107876.

[17] H. W. Yan, A. Narang, H. D. Tafti, G. G. Farivar, S. Ceballos and J. Pou, ”Minimizing Energy Storage Utilization in a Stand-Alone DC Microgrid Using Photovoltaic Flexible Power Control,” in IEEE Transactions on Smart Grid, vol. 12, no. 5, pp. 3755-3764, Sept. 2021, doi: 10.1109/TSG.2021.3073370.

[18] W. Dwiono, B. R. Trilaksono, T. D. Rachmildha and A. Rizqiawan, "Finite Control Sets Model Predictive Control (FCS-MPC) Implementation in PV Converter System for Maintaining The DC Bus Voltage," 2023 4th International Conference on High Voltage Engineering and Power Systems (ICHVEPS), Denpasar Bali, Indonesia, 2023, pp. 164-169, doi: 10.1109/ICHVEPS58902.2023.10257479.

[19] P. Karamanakos, T. Geyer and S. Manias, ”Direct Model Predictive Current Control Strategy of DC–DC Boost Converters,” in IEEE Journal of Emerging and Selected Topics in Power Electronics, vol. 1, no. 4, pp. 337-346, Dec. 2013, doi: 10.1109/JESTPE.2013.2279855.

[20] Z. Karami, Q. Shafiee, S. Sahoo, M. Yaribeygi, H. Bevrani and T. Dragicevic, ”Hybrid Model Predictive Control of DC–DC Boost Converters With Constant Power Load,” in IEEE Transactions on Energy Conversion, vol. 36, no. 2, pp. 1347-1356, June 2021, doi: 10.1109/TEC.2020.3047754.

[21] Dahono, Andriazis & Dahono, Pekik, “A Comparative Evaluation of Bidirectional Step-Up DC-DC Converters”. International Journal on Electrical Engineering and Informatics. 12. 388-397. 10.15676/ijeei.2020.12.2.14.

[22] C. Xue, W. Song, X. Wu and X. Feng, "A Constant Switching Frequency Finite-Control-Set Predictive Current Control Scheme of a Five-Phase Inverter With Duty-Ratio Optimization," in IEEE Transactions on Power Electronics, vol. 33, no. 4, pp. 3583-3594, April 2018, doi: 10.1109/TPEL.2017.2707440.

[23] R.B.A. Cunha, R.S. Inomoto, J.A.T. Altuna, F.F. Costa, S.G. Di Santo, A.J. Sguarezi Filho, Constant switching frequency finite control set model predictive control applied to the boost converter of a photovoltaic system, Solar Energy, Volume 189, 2019, Pages 57-66, ISSN 0038-092X, https://doi.org/10.1016/j.solener.2019.07.021.

[24] Y. Li, S. Sahoo, T. Dragičević, Y. Zhang and F. Blaabjerg, "Stability-Oriented Design of Model Predictive Control for DC/DC Boost Converter," in IEEE Transactions on Industrial Electronics, vol. 71, no. 1, pp. 922-932, Jan. 2024, doi: 10.1109/TIE.2023.3247785.

[25] Muqorobin, Anwar & Rachmildha, Tri & Haroen, Yanuarsyah & Rijanto, Estiko. “A Hybrid Controller for Boost Inverter: Modeling, Simulation, and Experimental Results”. International Journal on Electrical Engineering and Informatics. 13. 179-190. 10.15676/ijeei.2021.13.1.10.

Wakhyu Dwiono received the B.S degree from Electrical Engineering at the Universitas Diponegoro and Master’s degree from the Institut Teknologi Bandung, Indonesia, where he is currently pursuing the Doctoral degree in electrical engineering. His research interests include control systems and DC microgrid systems.

Bambang R. Trilaksono received the B.S degree from Electrical Engineering at the Institut Teknologi Bandung, Master’s and a Ph.D. degree from Electrical Engineering, Waseda University, Japan. Currently, he is a Professor in the Control and Computer System Research Group at the Institut Teknologi Bandung. His research interests include optimal control, robust control, intelligent control and systems, discrete event systems, control applications, robotics, and embedded control systems.

Tri Desmana Rachmildha He received B.Eng and M.Eng degrees in electrical engineering from Bandung Institute of Technology (ITB), Indonesia, in 1998 and 2002, respectively. He received Doctor Degree in Electrical Engineering from Joint PhD Supervision Program between Institut Nationale Polytechnique de Toulouse – Ecole Nationale Superieure d'Electrotechnique, d'Electronique, d'Informatique, d'Hydrolique, et de Telecommunication (INPT–ENSEEIHT, France) and School of Electrical Engineering and Informatics, Bandung Institute of Technology, Indonesia, in 2009. He is a researcher at Electrical Energy Conversion Research Laboratory, ITB. Since 2008, he is a lecturer at School of Electrical Engineering and Informatics ITB, Indonesia. His research interests include power electronics and electrical machinery. Dr. Tri Desmana Rachmildha can be contacted trides@konversi.ee.itb.ac.id and trides@gmail.com.

Arwindra Rizqiawan received the bachelor's and master's degrees from the Insititut Teknologi Bandung, Indonesia, in 2006 and 2008, respectively, and the Ph.D. degree from the Shibaura Institute of Technology, Japan, in 2012, all in electrical engineering. His current interests include power engineering, power electronics, and renewable energy. He is currently serving as an Assistant Professor with the School of Electrical Engineering and Informatics, Institut Teknologi Bandung. He is a certified Professional Engineer (IPM) in Indonesia by the Institution of Engineers Indonesia (PII), and an ASEAN Engineer by ASEAN Engineering Register.